Electronic Research Archive

https://www.aimspress.com/journal/era

ERA, 34(1): 31–47.
DOI: 10.3934/era.2026002
Received: 28 October 2025
Revised: 08 December 2025
Accepted: 23 December 2025
Published: 26 December 2025

Research article

Red blood cells as elastic surfaces: Cassini ovals, Helfrich shape equation, and biophysical regimes

Eugenio Aulisa, Magdalena Toda, Stone Fields and Erhan Güler*

Department of Mathematics and Statistics, Texas Tech University, Lubbock, TX 79409, USA

* **Correspondence:** Email: eguler@ttu.edu.

Abstract: Red blood cells (RBCs) are classically modeled as thin elastic surfaces governed by the Helfrich–Canham energy. Within the widely used axisymmetric framework, we provide what appears to be the first complete mathematical proof that Cassini ovals, except for the limiting round sphere, do *not* satisfy the Helfrich shape equation, even though they can approximate biconcave profiles over experimentally relevant parameter ranges. The argument proceeds by direct substitution of the Cassini meridian into the third-order reduced shape equation and yields an overdetermined algebraic system with no consistent solution for any nonzero Cassini eccentricity.

Beyond this structural result, we place the analysis in a broader biophysical and geometric context. We review typical bending and shear moduli, reduced-volume constraints, and the role of area and volume conservation; we explain the geometric meaning of the Helfrich parameters and their relation to the Willmore functional; we connect our formulation to bilayer-couple and area-difference-elasticity (ADE) models; and we outline practical routes to parameter inference from micropipette aspiration, flicker spectroscopy, and optical tweezers. We also discuss why the specific curvature structure of Cassini ovals is conceptually incompatible with Helfrich equilibria, indicate regimes in which Cassini profiles remain useful surrogates for geometric descriptors and for initializing PDE-based solvers, and summarize recent models based on constant bending-energy density. Finally, we identify extensions with spatially varying spontaneous curvature that may accommodate membrane heterogeneity and more complex RBC morphologies.

Keywords: generalized Willmore surface; Helfrich surface; shape equation; red blood cell; reduced volume; bilayer-couple; cytoskeleton; closed elastic surfaces

1. Introduction

Red blood cells (RBCs, erythrocytes) are the most abundant cells in human blood and are optimized for efficient gas transport under severe geometric constraints in microcirculation. In

physiological conditions, healthy mammalian RBCs exhibit a characteristic biconcave discoid shape: the diameter is about 7.5–8.5 μm, the rim thickness is roughly 2 μm, and the central thickness is about 1 μm. The surface area is approximately 130–150 μm^2, enclosing a volume of 80–100 μm^3. These geometric parameters are remarkably robust among healthy cells and provide important constraints for mathematical models.

Following the pioneering work of Helfrich [1], lipid bilayers are modeled as two-dimensional elastic surfaces embedded in $\mathbb{R}^3$, with an energy functional that penalizes mean-curvature deviations and incorporates spontaneous curvature. Red blood cell shapes were explained using curvature elasticity theory by Deuling and Helfrich [2]. This curvature elasticity framework was later extended to derive the shape equations for axisymmetric vesicles [3]. For closed vesicles of fixed topology, the Gaussian-curvature term contributes a topological constant and therefore does not appear in the local Euler–Lagrange equation; in particular, it does not enter the shape equation.

In [4], RBC profiles were modeled by Angelov and Mladenov using Cassini ovals, with estimates provided for geometric and energetic parameters. Similarly, Liu et al. [5] derived RBC shapes via minimization of total elastic surface energy. Light scattering by concave, peanut-shaped silver nanoparticles modeled on Cassini ovals was investigated by Hellmers et al. [6]. While Cassini ovals have been proposed as highly accurate descriptors of RBC profiles [4], their compatibility with the Helfrich–Canham shape equation has not been rigorously established. Relatedly, an outstanding doctoral thesis by Rodríguez Lázaro compares the RBC biconcave profile with a Cassini-oval parametrization and treats it as an acceptable approximation for light-scattering and rheological purposes [7, Pages 20–25].

The stability and second variation of the Helfrich energy for equilibrium membrane surfaces satisfying the reduced membrane equation were studied by Palmer and Pampano [8]. Recently, red blood cells were modeled as Helfrich surfaces with spherical topology by Aulisa et al. [9].

In this study, we prove that Cassini ovals, except for the limiting case of the round sphere, do not solve the shape equation. We have thoroughly reviewed the related literature, and it became apparent that a mathematically rigorous proof of this statement was never published in peer reviewed journals before.

Beyond the incompatibility result, several modeling questions arise naturally. How should one interpret the Helfrich parameters in biophysical terms? How does the Helfrich energy relate to the classical Willmore functional? How are the parameters estimated experimentally and how sensitive are predicted shapes to their values? And in what sense can Cassini ovals remain useful, despite not being exact equilibria? We address these questions by combining tools from differential geometry, variational calculus, and continuum mechanics.

Important Remark. The spontaneous curvature c_0 is often treated as a constant for homogeneous membranes. In practice, protein adsorption, lipid asymmetry, temperature, shear, and cytoskeletal coupling can make c_0 effectively space-dependent. We adopt the constant-c_0 model for analytical clarity and to enable comparison with the classical literature; we revisit non-constant c_0 in the Conclusion Section.

2. Background and methods

2.1. Biophysical background and parameter ranges

RBC membranes are composite structures: a lipid bilayer (bending-dominated) coupled to a spectrin-based cytoskeletal network (shear-dominated). Typical physiological values are

- effective bending modulus $\kappa \in (1-3)\times 10^{-19}$ J (roughly $25-75\,k_BT$, which represents the thermal energy scale, where k_B is the Boltzmann constant and T is the absolute temperature),
- in-plane shear modulus $\mu \in (4-12)\,\mu$N/m for the cytoskeleton,
- effective area compressibility $K_A \gg \mu$ (the membrane is nearly area-incompressible),
- cell diameter $\approx 7.5-8.5\,\mu$m, rim thickness $\approx 2\,\mu$m, central thickness $\approx 1\,\mu$m,
- surface area $\approx 130-150\,\mu\text{m}^2$, volume $\approx 80-100\,\mu\text{m}^3$.

Across normal donors, the *reduced volume*

$$v \;=\; \frac{V}{\frac{4\pi}{3}\left(\frac{A}{4\pi}\right)^{-3/2}}$$

typically lies near $v \approx 0.6$, a regime where unconstrained Helfrich vesicles exhibit biconcave discoid shapes. Bilayer-couple and area-difference-elasticity (ADE) models refine this picture by penalizing leaflet area difference and thereby shifting the biconcave↔prolate transition boundaries. Cytoskeletal models (e.g., Skalak or Neo-Hookean surface energies) superimpose in-plane shear elasticity, which becomes critical in tank-treading, shear flow, and large deformations. The mechanical and thermodynamic principles governing biomembranes were systematically developed in the seminal monograph by Evans and Skalak [10]. A comprehensive theoretical review of fluid membrane and vesicle configurations, including curvature elasticity and shape transformations, was provided by Seifert [11]. The relationship between the mechanical properties of red blood cell membranes, their molecular structure, and genetic defects was analyzed in detail by Mohandas and Evans [12].

Experimentally, κ can be inferred from flicker spectroscopy; μ from micropipette aspiration and optical tweezers; ΔP and λ from osmotic and aspiration protocols. These data enable meaningful priors and cross-validation for curvature models and for the shape equation fits discussed below.

2.2. Helfrich versus Willmore energy

For a closed membrane surface $M \subset \mathbb{R}^3$, the bending part of the Helfrich–Canham energy is

$$\Theta_{\text{bend}}(M) = \int_M \beta\,(2H - c_0)^2\,dS \;= 4\beta \int_M H^2\,dS \;- 4\beta c_0 \int_M H\,dS \;+ \beta c_0^2 \int_M dS.$$

When $c_0 = 0$ and $\lambda = 0$, the functional reduces to the classical *Willmore functional*

$$\mathcal{W}(M) = \int_M H^2\,dS,$$

whose critical points are known as *Willmore surfaces*, and have been studied extensively in differential geometry. Curvature-dependent variational functionals and the theory of p-Willmore energy were studied in detail in the doctoral thesis of Gruber [13]. Willmore-type energies and the

associated surfaces in space forms were investigated by Athukorallage et al. [14]. Foundational analytical techniques and classical results on minimal surfaces were systematically presented in the lecture notes by Nitsche [15]. A computational approach to the p-Willmore flow incorporating a conformal penalty was developed by Gruber and Aulisa [16].

From the RBC standpoint, the Willmore functional provides a natural reference model in which bending energy depends only on the square of the mean curvature. However, real membranes exhibit leaflet asymmetry and are subject to area and volume constraints; consequently, the full Helfrich energy is more appropriate.

In particular:

- the Willmore model ($c_0 = 0$, $\lambda = \Delta P = 0$) is scale-invariant and does not fix cell size or volume;
- the spontaneous curvature term c_0 and the tension/pressure terms $\lambda, \Delta P$ break this invariance and select specific shapes and sizes;
- extended models may add further contributions (bilayer-couple, ADE, shear elasticity) which, in many cases, can be reinterpreted as an effective shift in c_0 plus global constraints.

Thus, the Helfrich model can be viewed as a Willmore-type energy with additional lower-order terms reflecting physically relevant constraints. This viewpoint is useful both conceptually and technically.

2.3. First variation and the Helfrich shape equation

For a closed membrane surface $M \subset \mathbb{R}^3$ enclosing a region $\Omega(M)$, the Helfrich–Canham energy is defined as:

$$\Theta(M) = \int_M \beta(2H - c_0)^2 \, dS + \lambda \int_M dS + \Delta P \int_{\Omega(M)} dV, \tag{2.1}$$

alternatively referred to as the *Helfrich–Canham functional*. We have used the original notations of [1], where the surface, area and volume integrals are distinguished based on the integration element.

In this expression:

- $\beta > 0$ is the *bending rigidity* of the membrane;
- $c_0 \in \mathbb{R}$ is the *spontaneous curvature*, as introduced in [1, 3], and other foundational works;
- $H = -\frac{k_1+k_2}{2}$ is the *mean curvature* (also known as *Germain curvature*), where k_1 and k_2 are the principal curvatures;
- λ and ΔP are *Lagrange multipliers* enforcing constraints of constant surface area and enclosed volume, respectively. These correspond physically to *surface tension* and *osmotic pressure*.

The sign of H depends on the choice of surface orientation. Additionally, c_0 can take different signs in various physical contexts, depending on whether the membrane tends to bend inward or outward in the absence of external forces.

When $c_0 = 0$, the functional simplifies to the classical *Willmore functional*, and its critical points are known as *Willmore surfaces*.

It is important to note that, when defining this curvature functional, the Gaussian curvature $K = k_1 \cdot k_2$ may or may not appear under the first term of the integral. For a *closed* surface with *fixed topology*, the integral $\int_M K \, dS = 4\pi\chi(M)$ (by virtue of Gauss–Bonnet Theorem) is a topological constant.

A fundamental step in studying membrane shapes is computing the *first variation* of the functional under normal deformations of a one-parameter family of closed surfaces. Since the surface is closed,

Green's Theorem can be applied to derive the associated *Euler–Lagrange equation*. This equation characterizes the critical points of the Helfrich functional and is commonly referred to in the literature as the *shape equation*, *Helfrich equation*, or *Helfrich shape equation* ([1, 3, 17–20]):

$$2\Delta H + (2H - c_0)\left[2H^2 - 2K + c_0 H\right] + \bar{P} - 2\bar{\lambda}H = 0, \tag{2.2}$$

where the normalized parameters are defined by

$$\bar{P} := \frac{\Delta P}{\beta}, \qquad \bar{\lambda} := \frac{\lambda}{\beta}.$$

These nondimensional parameters are often used in the literature for convenience, except in cases where $\beta = 1$ is assumed.

Important Remark. The Helfrich shape equation is a nonlinear, fourth-order elliptic partial differential equation which poses substantial analytical challenges. To make the problem more tractable, researchers commonly assume axial symmetry, which allows significant simplification. This axisymmetric model has been widely adopted in the literature.

2.4. Shape equation for the particular case of axisymmetric surfaces with spherical topology

Let $X : D \to \mathbb{R}^3$ be a smooth surface immersion in $\mathbb{R}^3$, where the domain D is defined as $(0, \alpha) \times (0, 2\pi)$, an open, simply connected subset of the plane. We use the following axisymmetric parametrization:

$$X(s, v) = (r(s)\cos v,\ r(s)\sin v,\ z(s)),$$

where s is the arclength along the profile curve $(r(s), z(s))$. Rotating this curve around the z-axis generates the surface. Such a surface of revolution is called an *axisymmetric surface*.

We study RBC shapes modeled by closed axisymmetric surfaces, where s denotes arclength, r is the radial coordinate (distance from the z-axis), and ψ is the angle between the profile curve's tangent vector and the horizontal axis, measured counterclockwise from the horizontal axis.

This profile can equivalently be described using the function $\psi = \psi(r)$, where ψ is the *tangent angle* at the point with rotation radius r. By definition:

$$\psi(r) = -\arctan\left(\frac{dz}{dr}\right). \tag{2.3}$$

The coordinate functions $z(s)$ and $r(s)$ satisfy the differential relationships:

$$\frac{dz}{ds} = -\sin\psi, \qquad \frac{dr}{ds} = \cos\psi, \tag{2.4}$$

which imply

$$\frac{dz}{dr} = -\tan\psi.$$

The signs of these expressions are consistent with our chosen angle orientation: ψ is measured counterclockwise from the horizontal axis, as illustrated in Figure 1.

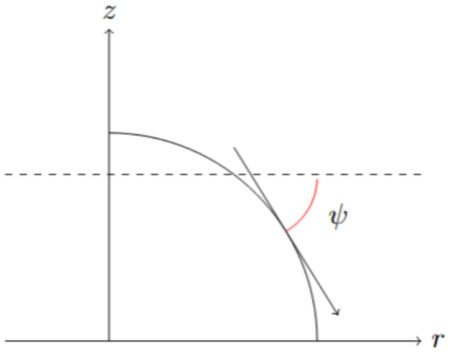

Figure 1. Axisymmetric parametrization: r is the rotation radius and $\psi(r)$ is the tangent angle.

Using this axisymmetric frame, the curvatures can be re-expressed along the profile curve $z(r)$. Following the formulations in [18], we define:

$$H = -\frac{k_1 + k_2}{2} = -\frac{1}{2}\left(\cos\psi\frac{d\psi}{dr} + \frac{\sin\psi}{r}\right), \tag{2.5}$$

$$K = k_1 k_2 = \cos\psi\sin\psi \cdot \frac{1}{r} \cdot \frac{d\psi}{dr}, \tag{2.6}$$

where $\psi(s)$ is again the angle between the profile curve tangent and the horizontal direction.

Note the minus sign convention shown for the mean curvature is more common in physics, mechanics and biophysics, while mathematicians usually prefer the mean curvature to be defined by the arithmetic mean of the principal curvatures. A change of orientation on the surface M will result in a change in sign for the mean curvature.

In our work, we follow [17] and [18], who unified various shape equations appearing in earlier studies. We restrict our attention to axisymmetric surfaces with spherical topology (i.e., genus zero). The shape equation discussed below applies specifically to this setting and does not hold for surfaces of higher genus or for non-axisymmetric cases.

The *shape equation* represents the Euler–Lagrange equation $\mathcal{H}(\psi) = 0$ corresponding to the Helfrich–Canham functional, written in terms of the angle ψ introduced above.

As seen in [17], a third-order formulation of the Helfrich shape equation is given by:

$$\begin{aligned}\mathcal{H} = &-\cos^3\psi\frac{d^3\psi}{dr^3} + 4\sin\psi\cos^2\psi\frac{d^2\psi}{dr^2} - \cos\psi\left(\sin^2\psi - \frac{1}{2}\cos^2\psi\right)\left(\frac{d\psi}{dr}\right)^3\\ &+ \frac{7\sin\psi\cos^2\psi}{2r}\left(\frac{d\psi}{dr}\right)^2 - \frac{2\cos^3\psi}{r}\frac{d^2\psi}{dr^2}\\ &+ \left(\frac{c_0^2}{2} - \frac{2c_0\sin\psi}{r} + \frac{\sin^2\psi}{2r^2} + \bar{\lambda} - \frac{\sin^2\psi - \cos^2\psi}{r^2}\right)\cos\psi\frac{d\psi}{dr}\\ &+ \bar{P} + \bar{\lambda}\sin\psi - \frac{\sin^2\psi}{2r^3} + \frac{c_0^2\sin\psi}{2r} - \frac{\sin\psi\cos^2\psi}{r^3} = 0.\end{aligned}$$

This expression can be unwieldy, and several methods exist to simplify it depending on the chosen parameterization. In the case of axisymmetric surfaces with spherical topology, the following simplified form of the shape equation is obtained (see [17–19]):

$$\mathcal{H} = \cos^2\psi\frac{d^2\psi}{dr^2} - \frac{\sin\psi\cos\psi}{2}\left(\frac{d\psi}{dr}\right)^2 - \frac{\sin\psi}{2r^2\cos\psi} - \frac{\sin\psi\cos\psi}{2r^2} - \frac{c_0^2\sin\psi}{2\cos\psi} + \frac{\cos^2\psi}{r}\frac{d\psi}{dr} - \frac{c_0\sin^2\psi}{r\cos\psi} - \frac{\bar{P}}{2}\frac{r}{\cos\psi} - \bar{\lambda}\frac{\sin\psi}{\cos\psi} = 0. \tag{2.7}$$

3. Results and discussion

3.1. Cassini ovals versus the shape equation

Cassini ovals have been investigated in multiple papers, including [4]. Cassini ovals are a class of algebraic curves associated with toric sections, which in the present notation can be represented as

$$z(r) = \pm\sqrt{\sqrt{4a^2r^2 + c^4} - a^2 - r^2}, \tag{3.1}$$

where $a, c \in \mathbb{R}$. It is convenient to view a, c through the ratio that characterizes the Cassini ovals. We write $e = \frac{c}{a}$ for the eccentricity; its multiplicative inverse $\epsilon = \frac{a}{c}$ is often called the biconcavity of a Cassini oval.

Rewriting (3.1) in terms of biconcavity and rescaling, we obtain

$$z(r) = \pm\sqrt{\sqrt{4\epsilon^2r^2 + 1} - \epsilon^2 - r^2}. \tag{3.2}$$

The formulas above correspond to the classical Cassini family, which has been widely used as an analytic surrogate for biconcave RBC profiles; in this paper they are not proposed as Helfrich solutions but rather are shown rigorously not to satisfy the Helfrich shape equation, except in the limiting spherical case

One checks that $0 \le \epsilon < 1$ implies that the argument under the outer square root,

$$\sqrt{4\epsilon^2r^2 + 1} - \epsilon^2 - r^2, \tag{3.3}$$

is nonnegative for $0 \le r \le \sqrt{1+\epsilon^2}$, and is nonnegative for $\sqrt{-1+\epsilon^2} \le r \le \sqrt{1+\epsilon^2}$ when $\epsilon \ge 1$. We must then restrict our domain for derivatives to exist, i.e., require that (3.3) be strictly positive. Letting $\epsilon \ge 0$, the domain of definition is:

$$D := \begin{cases} 0 \le r < \sqrt{1+\epsilon^2} & \text{for} \quad 0 \le \epsilon < 1, \\ \sqrt{-1+\epsilon^2} < r < \sqrt{1+\epsilon^2} & \text{for} \quad \epsilon \ge 1. \end{cases} \tag{3.4}$$

The main result of the current work is stated and proved below.

Theorem 3.1. *For $\epsilon > 0$, Cassini ovals used as axisymmetric profile curves do not satisfy the shape equation* (2.7).

Proof. First, we assume that the Cassini oval satisfies the shape equation. Thus, any profile curve must satisfy

$$\mathcal{H} = \cos^2\psi\frac{d^2\psi}{dr^2} - \frac{\sin\psi\cos\psi}{2}\left(\frac{d\psi}{dr}\right)^2 - \frac{\sin\psi}{2r^2\cos\psi} - \frac{\sin\psi\cos\psi}{2r^2} + \frac{\cos^2\psi}{r}\frac{d\psi}{dr} - \frac{c_0^2\sin\psi}{2\cos\psi} - \frac{c_0\sin^2\psi}{r\cos\psi} - \frac{\bar{P}}{2}\frac{r}{\cos\psi} - \bar{\lambda}\frac{\sin\psi}{\cos\psi} = 0.$$

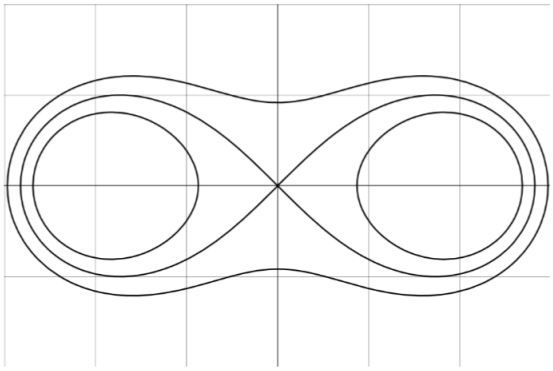

Figure 2. Cassini ovals with $e = 0.9$, $e = 1.0$, and $e = 1.1$; generated by authors with *Mathematica*.

Cassini ovals for different values of the parameter e are presented in Figure 2. We will derive a contradiction by reframing the equation in terms of the Cassini ovals and showing that they do not satisfy the shape equation. By definition, we have that $\psi(r) = -\arctan\left(\frac{dz}{dr}\right)$. Using Eq (3.2) and substituting $u(r) = z'(r)$ yields the following expression:

$$\mathcal{H} = \frac{-5u(u')^2}{2(1+u^2)^3} + \frac{u''}{(1+u^2)^2} - \frac{u}{2r^2}\left(1 + \frac{1}{1+u^2}\right) + \frac{1}{r}\frac{u'}{(1+u^2)^2} - \frac{c_0^2}{2}u - \frac{c_0u^2}{r\sqrt{1+u^2}} - \frac{\bar{P}r}{2}\sqrt{1+u^2} - \bar{\lambda}u.$$

We explicitly compute the first derivative of $z(r)$:

$$u(r) := z'(r) = \frac{r}{2\sqrt{\sqrt{1+4\epsilon^2r^2} - \epsilon^2 - r^2}}\left(\frac{4\epsilon^2}{\sqrt{1+4\epsilon^2r^2}} - 2\right), \tag{3.5}$$

and substitute as appropriate. Under the assumption that $\sqrt{1+4\epsilon^2r^2} - \epsilon^2 - r^2 > 0$, we simplify the expression and obtain

$$\mathcal{H}\left(\sqrt{1+4r^2\epsilon^2} - \epsilon^2\right)^3\left(\sqrt{1+4r^2\epsilon^2} - r^2 - \epsilon^2\right)^{3/2} = 0$$

for all $r \in D$. With the aid of symbolic computation (e.g., Mathematica), substituting and simplifying lead to the following equation

$$\mathcal{H}_1 + \frac{\mathcal{H}_2}{\sqrt{1+4r^2\epsilon^2}} + \mathcal{H}_3\sqrt{-\epsilon^2+\sqrt{1+4r^2\epsilon^2}} + \mathcal{H}_4\sqrt{\frac{-\epsilon^2+\sqrt{1+4r^2\epsilon^2}}{1+4r^2\epsilon^2}} = 0, \tag{3.6}$$

with

$$\begin{aligned}\mathcal{H}_1 =& \frac{c_0^2 r}{2} - 8r\epsilon^2 + \frac{13}{2}c_0^2 r^3\epsilon^2 - 6r^5\epsilon^2 + 7c_0^2 r\epsilon^4 - 72r^3\epsilon^4 + 18c_0^2 r^5\epsilon^4 - 10r^7\epsilon^4 - 24r\epsilon^6 + \frac{63}{2}c_0^2 r^3\epsilon^6 \\ & - 114r^5\epsilon^6 + \frac{9}{2}c_0^2 r\epsilon^8 - 60r^3\epsilon^8 + r\bar{\lambda} + 13r^3\epsilon^2\bar{\lambda} + 14r\epsilon^4\bar{\lambda} + 36r^5\epsilon^4\bar{\lambda} + 63r^3\epsilon^6\bar{\lambda} + 9r\epsilon^8\bar{\lambda}, \end{aligned} \tag{3.7}$$

$$\begin{aligned}\mathcal{H}_2 =& -\frac{1}{2}c_0^2 r^3 - 3c_0^2 r\epsilon^2 + 14r^3\epsilon^2 - 4c_0^2 r^5\epsilon^2 + 24r\epsilon^4 - \frac{57}{2}c_0^2 r^3\epsilon^4 + 84r^5\epsilon^4 - 8c_0^2 r^7\epsilon^4 - 8c_0^2 r\epsilon^6 \\ & + 158r^3\epsilon^6 - 66c_0^2 r^5\epsilon^6 + 108r^7\epsilon^6 + 8r\epsilon^8 - 33c_0^2 r^3\epsilon^8 + 236r^5\epsilon^8 - c_0^2 r\epsilon^{10} + 24r^3\epsilon^{10} - r^3\bar{\lambda} \\ & - 6r\epsilon^2\bar{\lambda} - 8r^5\epsilon^2\bar{\lambda} - 57r^3\epsilon^4\bar{\lambda} - 16r^7\epsilon^4\bar{\lambda} - 16r\epsilon^6\bar{\lambda} - 132r^5\epsilon^6\bar{\lambda} - 66r^3\epsilon^8\bar{\lambda} - 2r\epsilon^{10}\bar{\lambda}, \end{aligned} \tag{3.8}$$

$$\begin{aligned}\mathcal{H}_3 =& -c_0 r + \frac{1}{2}\bar{P}r^3 + 2\bar{P}r\epsilon^2 - 14c_0 r^3\epsilon^2 + 2\bar{P}r^5\epsilon^2 - 19c_0 r\epsilon^4 \\ & + \frac{19}{2}\bar{P}r^3\epsilon^4 - 40c_0 r^5\epsilon^4 + 2\bar{P}r\epsilon^6 - 88c_0 r^3\epsilon^6 - 16c_0 r\epsilon^8, \end{aligned} \tag{3.9}$$

$$\begin{aligned}\mathcal{H}_4 =& -\frac{1}{2}\bar{P}r + c_0 r^3 + 7c_0 r\epsilon^2 - \frac{11}{2}\bar{P}r^3\epsilon^2 + 8c_0 r^5\epsilon^2 - 3\bar{P}r\epsilon^4 + 69c_0 r^3\epsilon^4 - 14\bar{P}r^5\epsilon^4 \\ & + 16c_0 r^7\epsilon^4 + 25c_0 r\epsilon^6 - \frac{25}{2}\bar{P}r^3\epsilon^6 + 164c_0 r^5\epsilon^6 - \frac{1}{2}\bar{P}r\epsilon^8 + 104c_0 r^3\epsilon^8 + 4c_0 r\epsilon^{10}. \end{aligned} \tag{3.10}$$

Since Eq (3.6) must be satisfied for all r in the domain D, the four functions

$$1, \quad (1+4\epsilon^2 r^2)^{-1/2}, \quad \sqrt{-\epsilon^2+\sqrt{1+4\epsilon^2 r^2}}, \quad \sqrt{\frac{-\epsilon^2+\sqrt{1+4\epsilon^2 r^2}}{1+4\epsilon^2 r^2}}$$

are linearly independent and we require that

$$\mathcal{H}_1(r) \equiv 0, \quad \mathcal{H}_2(r) \equiv 0, \quad \mathcal{H}_3(r) \equiv 0, \quad \mathcal{H}_4(r) \equiv 0.$$

It suffices to show that the equation $\mathcal{H}_3(r) \equiv 0$ leads to a contradiction. Collecting terms with the same monomials in r,

$$\mathcal{H}_3(r) = r^5\left(2\bar{P}\epsilon^2 - 40c_0\epsilon^4\right) + r^3\left(\frac{\bar{P}}{2} - 14c_0\epsilon^2 + \frac{19\bar{P}\epsilon^4}{2} - 88c_0\epsilon^6\right) + r\left(-c_0 + 2\bar{P}\epsilon^2 - 19c_0\epsilon^4 + 2\bar{P}\epsilon^6 - 16c_0\epsilon^8\right).$$

Since this polynomial must vanish for all r, its coefficients must vanish, and we obtain the algebraic system

$$\begin{cases} 2\bar{P}\epsilon^2 - 40c_0\epsilon^4 = 0, \\ \dfrac{\bar{P}}{2} - 14c_0\epsilon^2 + \dfrac{19\bar{P}\epsilon^4}{2} - 88c_0\epsilon^6 = 0, \\ -c_0 + 2\bar{P}\epsilon^2 - 19c_0\epsilon^4 + 2\bar{P}\epsilon^6 - 16c_0\epsilon^8 = 0. \end{cases} \tag{3.11}$$

The first equation gives $\bar{P} = 20c_0\epsilon^2$. Substituting into the second and third equations yields

$$\epsilon = \left(\frac{2}{51}\right)^{1/4} \quad \text{and} \quad \epsilon = \frac{1}{2}\left(\frac{1}{3}(-21 + \sqrt{537})\right)^{\frac{1}{4}},$$

respectively. This is a contradiction since ϵ would take on two different values, yielding two different Cassini ovals. It follows that for $\epsilon > 0$ Cassini ovals do not satisfy the shape equation (2.7).

Important Remark. Although Cassini ovals are not true solutions of the Helfrich shape equation (except in the spherical limit), they remain useful as biophysically relevant approximations. The doctoral thesis by Rodríguez Lázaro previously mentioned explicitly shows that the Cassini profile reproduces measured RBC meridians within experimental tolerance and can therefore be employed as an analytic surrogate in optical modeling of light scattering and in rheological contexts where only gross geometric descriptors are required [7, Pages 20–25]. Similar approximations have also been used in forward optical models of RBC diffraction and tomography, where closed-form analytic surfaces are advantageous.

3.2. Conceptual explanation of the incompatibility

The algebraic proof above shows rigorously that Cassini ovals cannot solve the Helfrich shape equation for any nonzero biconcavity parameter ϵ. It is instructive to complement this with a more geometric explanation.

The central feature of Cassini ovals in the present parametrization is the presence of two nested square roots in (3.2). As a consequence, the curvature invariants $H(r)$ and $K(r)$ generated by (3.2) have a very specific functional dependence on r: they belong to a finite-dimensional space of functions spanned by combinations of

$$\sqrt{1 + 4\epsilon^2 r^2}, \quad \frac{1}{\sqrt{1 + 4\epsilon^2 r^2}}, \quad \sqrt{\sqrt{1 + 4\epsilon^2 r^2} - \epsilon^2 - r^2},$$

and rational multiples of these in r.

On the other hand, the Helfrich shape equation (2.2) couples H and K in a nonlinear way that mixes these structures. Roughly speaking, the equation enforces a delicate balance among:

- the Laplacian of the mean curvature, ΔH, which is a second-order surface derivative and typically generates more complicated radial dependencies;
- the cubic nonlinearity in H, via the term $(2H - c_0)(2H^2 - 2K + c_0 H)$;
- the linear contributions of H and constants, scaled by $\bar{\lambda}$ and $\bar{P}$.

For generic axisymmetric surfaces, the competition among these contributions yields a large function space of possible profiles. However, for Cassini ovals the functional degrees of freedom are severely restricted by the nested radical structure. As a result, only in the special case $\epsilon = 0$ (where the nested radicals collapse to polynomials in r) can the shape equation be satisfied.

Another way to phrase this observation is the following: the Helfrich equation imposes local curvature constraints at each point on the surface, including at the rim and at the center of the biconcavity. For Cassini ovals, the curvature at these locations is rigidly tied to the global algebraic

structure of the curve. The apparent geometric similarity between Cassini ovals and real RBC shapes is thus insufficient: the local curvature constraints required by Helfrich equilibria are too restrictive to be accommodated by the Cassini family, except in the spherical limit.

3.3. Round spheres as limiting case solutions of the shape equation

Though Cassini ovals as a profile curve are not solutions to the shape equation for $\epsilon > 0$, it can be shown that for the limit case of $\epsilon = 0$ the Cassini ovals do satisfy (2.7). The easiest way this can be verified is by considering a sphere Σ with radius a. Letting $k_1 = k_2 = H = 1/a$ or $k_1 = k_2 = H = -1/a$, we substitute directly into the Helfrich shape equation (2.2).

In [9], the authors have shown that $\psi = a \arcsin r$ and $\psi = -a \arcsin r$ represent solutions that can be verified directly in the axisymmetric shape equation that explicitly depends on ψ. More precisely, the following result was proven:

Theorem 3.2. (I) *For $\psi = a \arcsin r$, in order for spherical solutions to exist, the surface Σ must satisfy the following constraint on the parameters c_0, $\bar{P}$, $\bar{\lambda}$:*

$$\bar{P}a^2 + [c_0^2 + 2\bar{\lambda}]a + 2c_0 = 0. \tag{3.12}$$

(II) *For $\psi = -a \arcsin r$, in order for spherical solutions to exist, the surface Σ must satisfy the following constraint on the parameters c_0, $\bar{P}$, $\bar{\lambda}$:*

$$\bar{P}a^2 - [c_0^2 + 2\bar{\lambda}]a + 2c_0 = 0. \tag{3.13}$$

If we impose the condition $\epsilon = 0$ on a Cassini oval, then (3.2) reduces to a circle, whose body of revolution is a round sphere. Based on the previous theorem, we conclude that Cassini ovals satisfy the shape equation only for $\epsilon = 0$, namely the spherical case.

3.4. Dimensionless formulation and reduced volume

For comparison across cell sizes and species, it is natural to non-dimensionalize lengths by $\ell = (A/4\pi)^{1/2}$, set $\tilde{r} = r/\ell$, and scale curvatures by ℓ^{-1}. Let $\tilde{H} = \ell H$, $\tilde{c}_0 = \ell c_0$, and retain $(\bar{\lambda}, \bar{P})$. Then (2.2) reads

$$2\tilde{\Delta}\tilde{H} + (2\tilde{H} - \tilde{c}_0)(2\tilde{H}^2 - 2\tilde{K} + \tilde{c}_0\tilde{H}) + \bar{P} - 2\bar{\lambda}\,\tilde{H} = 0,$$

subject to the reduced-volume constraint v and (if used) an ADE constraint proportional to the leaflets' area difference. In this setting, Cassini profiles can be judged not only by PDE residuals but also by deviations in (A, V) and v, which are measurable to high accuracy.

3.5. Relation to bilayer-couple and ADE models

The RBC membrane is a lipid *bilayer* with two monolayers (outer/inner) separated by a small half-thickness h. Because lipid numbers in the two leaflets may differ and flip-flop is slow, the *area difference*

$$\Delta A \;\equiv\; A_{\text{outer}} - A_{\text{inner}}$$

is effectively constrained on experimental time scales. For gently curved membranes with small h, one has the geometric approximation

$$\Delta A \;\approx\; 2h \int_M 2H\, dA,$$

so the leaflet area difference is controlled by the (global) integral of the mean curvature.

Area-Difference Elasticity (ADE) augments the Helfrich energy with a quadratic penalty that keeps ΔA near a preferred value ΔA_0 (set by lipid asymmetry):

$$\mathcal{F}_{\mathrm{ADE}} = \frac{k_\Delta}{2}\left(\Delta A - \Delta A_0\right)^2 = \frac{k_\Delta}{2}\left(2h\int_M 2H\,dA - \Delta A_0\right)^2,$$

where $k_\Delta > 0$ is an area-difference modulus. This term is *nonlocal* (it depends on a surface integral) and couples the shape globally through $\int 2H\,dA$.

In the *bilayer-couple* hypothesis, ΔA is treated as a hard constraint enforced by a Lagrange multiplier. ADE replaces this by a soft quadratic penalty around ΔA_0. In both cases, the variation introduces one extra global parameter (the Lagrange multiplier in bilayer–couple, or $q := k_\Delta(\Delta A - \Delta A_0)$ in ADE) that enters the local shape equation as an additive term linear in H. Equivalently, we may recast the local equation as a Helfrich equation with an effective spontaneous curvature $c_0^{\mathrm{eff}} = c_0 - \alpha\, q$ (for a constant α set by the chosen nondimensionalization), plus a global closure condition that determines q from ΔA_0.

Because ADE effectively shifts the preferred curvature, it moves the phase boundaries on the $(\tilde{c}_0, v)$ diagram (dimensionless spontaneous curvature vs. reduced volume). In practice this enlarges the parameter region where biconcave discocytes are energy-minimizing, consistent with RBC observations.

Our nonexistence result for Cassini meridians does not hinge on whether such a linear-in-H term is present. The contradiction we derive comes from the specific r-dependence produced when the Cassini profile is substituted into the axisymmetric differential operator in (2.7). Introducing a single additional constant (from ADE or bilayer–couple) cannot remove that functional mismatch for all r. Consequently, Cassini ovals remain non-solutions generically even under ADE. Nevertheless, because ADE shifts the effective curvature preference, there are parameter sets $(\tilde{c}_0, v, \mathrm{ADE})$ where the true Helfrich/ADE solution is close to a Cassini profile; in such regimes, Cassini curves can still serve as accurate approximations and useful initial guesses for solvers.

3.6. Parameter inference and use as approximations

Even when Cassini ovals are not exact solutions, they can be valuable surrogates. Some important aspects to consider are:

- *Geometric fits.* Cassini parameters can match diameter, rim/center thickness, and reduced volume within experimental error, yielding closed-form meridians useful for initialization and for rapid forward models (e.g., in optics and rheology).
- *Inverse problems.* Starting from Cassini fits, one can continue in $(\bar{P}, \bar{\lambda}, c_0)$ via a Newton or shooting scheme to converge to exact (2.7) solutions; this often improves robustness compared with random initializations.
- *Uncertainty quantification.* Comparing Cassini-based observables (area, volume, curvature histograms) with data-derived quantities (from flicker spectra or confocal reconstructions) provides residual-based diagnostics for model selection (Helfrich vs. ADE vs. shear-coupled) and for parameter sensitivity.
- *Alternative solution methods.* Beyond direct substitution, one may solve the axisymmetric ODE (2.7) using shooting methods, numerical continuation, or finite-element discretizations.

Cassini ovals can serve as initial guesses in these schemes, after which the profile is iteratively adjusted until the shape equation and global constraints are satisfied.

3.7. Recent RBC model based on constant energy density

Recent progress in the analytical and numerical modeling of biconcave discoid shapes, specifically red blood cell (RBC) profiles, has been made by Gonzalez et al. [20], including one of the present contributors. An axisymmetric RBC surface of revolution generated from the analytic profile given by ODE solutions is presented in Figure 3. We summarize these developments and further disseminate their implications for the current study.

Assuming that the bending energy density at every point on the RBC surface is proportional to the average squared deviation of the normal curvature from a reference curvature, denoted by $\langle(\kappa - \mathring{k})^2\rangle$, and that this energy density remains constant over the entire surface, the authors derived a differential equation governing the cross-sectional profile of an axisymmetric RBC. The profile is symmetric with respect to both the rotational axis and the equatorial plane. This differential equation, being quadratic in the first derivative, admits two distinct solution branches.

These two branches jointly define the full RBC profile. The inner region, from the cell center to the inflection point, corresponds to the first solution, which has a monotonically increasing slope starting from zero, ensuring regularity at the center. The outer region, extending from the inflection point to the cell's periphery, corresponds to the second solution, characterized by a monotonically decreasing slope. At the inflection point, the two solutions are found to extend each other regularly.

Two distinct cases are analyzed: one without spontaneous curvature and one incorporating it. The results indicate that only the model including spontaneous curvature can accurately reproduce the observed geometric parameters of real RBCs. In this refined model, the central parts of the RBC (bounded by upper and lower inflection circles) are described as a spherical cap and cup, respectively. Beyond these inflection points, the RBC surface transitions into a toroidal segment, whose cross-section approximates an elliptical arc. This geometric framework allows for accurate approximations of the cell's surface area and enclosed volume.

If the bending energy density is assumed to be a linear combination of the Gaussian curvature and the sum of the squares of the principal curvatures, and is also assumed constant, the resulting variational functional becomes equivalent to one with constant mean curvature H. By solving the profile differential equation for two different constant values of H (one from the cell center to the inflection point, and the other from the inflection point to the outer edge), the resulting shape closely matches real RBC geometry. This was demonstrated analytically, numerically, and experimentally.

The two values correspond to $(H - \mathring{k})^2 = a^2$, effectively modeling a constant bending energy density proportional to the square of the adjusted mean curvature.

In this formulation, the inner regions of the RBC surface (near the poles) again form a cup and cap, while the outer region resembles a nodoid surface. Models incorporating spontaneous curvature $\mathring{k}$ can therefore successfully replicate the RBC profile. In all cases, two distinct analytic expressions for the vertical coordinate z as a function of the radial coordinate x describe the geometry: one for the region from the center to the inflection point, and one from the inflection point to the periphery.

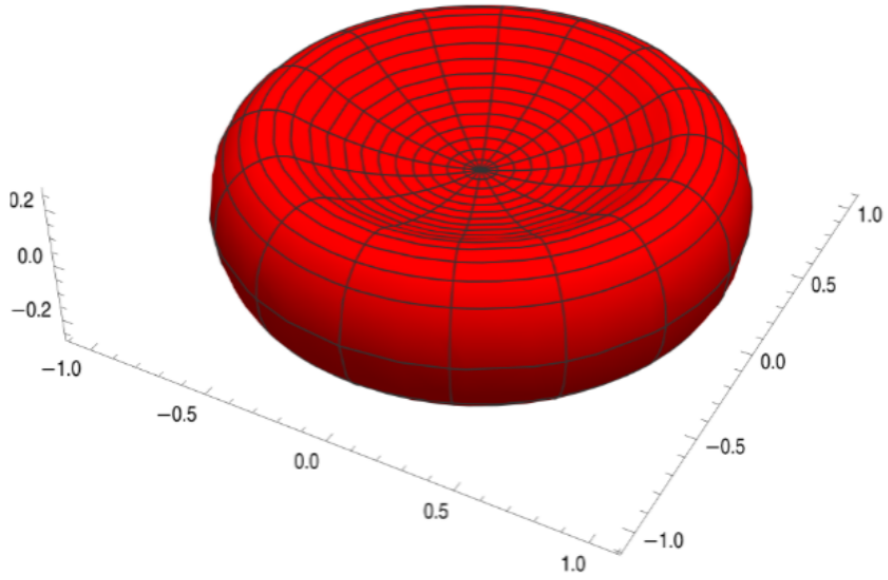

Figure 3. Axisymmetric RBC surface of revolution generated from the analytic profile given by ODE solutions, computed by the authors under the condition $H = \mathring{k} \pm a$; see [20].

4. Conclusions

We have shown that Cassini ovals—despite their successful use as analytic surrogates for RBC meridians—cannot be exact solutions of the classical Helfrich shape equation, except in the limiting spherical case. Our proof uses the standard axisymmetric reduction, expresses the shape equation in terms of the meridional slope, and analyzes the resulting functional identity. The nested radical structure of the Cassini profile leads to an overdetermined algebraic system whose only potential solutions for the biconcavity parameter ϵ are inconsistent, thus ruling out non-spherical Cassini equilibria.

From a modeling standpoint, Cassini ovals remain valuable *approximate* descriptors of RBC shapes. They can reproduce measured meridians and geometric quantities (area, volume, reduced volume) with high accuracy and provide convenient closed-form expressions for optics and rheology. However, they should not be interpreted as exact Helfrich equilibria. When a Helfrich (or extended) model is used as the governing PDE, Cassini shapes necessarily carry a nonzero residual. This residual can itself be exploited as a diagnostic quantity for model selection or parameter estimation.

Besides the limiting case $\epsilon = 0$, there are no straightforward Cassini-based solutions ψ that can simultaneously satisfy the shape equations and provide appropriate exact equilibria for RBCs. However, for cells whose chemical and physical properties vary significantly from point to point, it may be possible to consider non-constant spontaneous curvature and still satisfy (2.2) and (2.7).

In general, the spontaneous curvature c_0 appearing in the Helfrich–Canham energy is assumed to be constant. This assumption is mathematically convenient and often biologically reasonable when the membrane is homogeneous. However, real biological membranes can exhibit spatial variations in

curvature preferences due to factors such as protein distributions, lipid composition, or interactions with cytoskeletal elements. To capture such heterogeneity, one can consider c_0 as a function of the radial coordinate r, i.e., $c_0 = c_0(r)$.

In the axisymmetric setting, the shape equation involves terms that depend explicitly on c_0 and its spatial derivatives. When c_0 is non-constant, the equation gains additional terms involving $\frac{dc_0}{dr}$, which can significantly alter the solution landscape. These modifications may lead to new equilibrium shapes that cannot be obtained under the assumption of constant c_0.

Nonetheless, by prescribing specific functional forms for $c_0(r)$, one can obtain analytical or numerical solutions. For instance, the choice

$$c_0(r) = C_0 \cos^2\left(\frac{\pi r}{2r_0}\right)$$

has been proposed to model localized curvature-inducing effects, such as protein adsorption. This profile ensures smoothness and symmetry about the membrane midplane ($r = 0$) and vanishes at the membrane edge ($r = r_0$), consistent with physical constraints.

In this context, it is natural to investigate whether such non-constant $c_0(r)$ profiles might accommodate Cassini-like or related meridians that satisfy the axisymmetric shape equation. This represents a promising direction for modeling red blood cell shapes beyond the classical biconcave disc, especially when additional biophysical constraints are imposed. We leave a detailed analysis of spatially varying spontaneous curvature and its interplay with Cassini-type parametrizations for future work.

Author contributions

Eugenio Aulisa: Conceptualization, visualization, investigation, software, writing–original draft, writing–review and editing, supervision, funding acquisition; Magdalena Toda: Conceptualization, visualization, investigation, software, writing–original draft, writing–review and editing, supervision; Stone Fields: Software, investigation, writing–review and editing, formal analysis; Erhan Güler: Software, investigation, writing–review and editing, formal analysis. All authors have read and approved the final version of the manuscript for publication.

Use of AI tools declaration

The authors declare they have not used Artificial Intelligence (AI) tools in the creation of this article, except for Grammarly to correct linguistic and typographical errors.

Acknowledgments

We thank our colleagues A. Pampano, I. Mladenov and R. Gonzalez for their useful suggestions regarding the theoretical background of elastic surfaces. We benefited from extensive discussions on the mechanics of biomembranes and red blood cell shapes with researchers in mechanical engineering and biophysics.

Conflict of interest

The authors declare that they have no known competing financial interests or personal relationships that could have appeared to influence the work reported in this paper.

References

1. W. Helfrich, Elastic properties of lipid bilayers: Theory and possible experiments, *Z. Naturforsch. C*, **28** (1973), 693–703. https://doi.org/10.1515/znc-1973-11-1209
2. H. J. Deuling, W. Helfrich, Red blood cell shapes as explained on the basis of curvature elasticity, *Biophys. J.*, **16** (1976), 861–869. https://doi.org/10.1016/S0006-3495(76)85736-0
3. J. G. Hu, Z. C. Ou-Yang, Shape equations of axisymmetric vesicles, *Phys. Rev. E*, **47** (1993), 461–467. https://doi.org/10.1103/PhysRevE.47.461
4. B. Angelov, I. Mladenov, On the geometry of red blood cell, *Geom. Integrability Quantization*, **1** (2000), 27–46. https://doi.org/10.7546/giq-1-2000-27-46
5. Q. Liu, H. Zhou, J. Liu, Z. C. Ou-Yang, Spheres and prolate and oblate ellipsoids from an analytical solution of the spontaneous-curvature fluid-membrane model, *Phys. Rev. E*, **60** (1999) 3227–3233. https://doi.org/10.1103/PhysRevE.60.3227
6. J. Hellmers, N. Riefler, T. Wriedt, Y. Eremin, Light scattering simulation by concave, peanut-shaped silver nanoparticles modeled on Cassini-ovals, in *Proceedings of the International Conference on Electromagnetic Light Scattering (ICHMT)*, (2007), 53–56. https://doi.org/10.1615/ICHMT.2007.ConfElectromagLigScat.160
7. G. Rodríguez-Lázaro, *Red Blood Cell Mechanics: From Membrane Elasticity to Blood Rheology*, Ph.D. Thesis, Universitat de Barcelona, 2014.
8. B. Palmer, A. Pampano, Stability of membranes, *J. Geom. Anal.*, **34** (2024), 328. https://doi.org/10.1007/s12220-024-01767-7
9. E. Aulisa, S. Fields, M. Toda, Red blood cells as Helfrich surfaces with spherical topology, preprint, arXiv:2507.21010.
10. E. Evans, R. Skalak, *Mechanics and Thermodynamics of Biomembranes*, CRC Press, 1980.
11. U. Seifert, Configurations of fluid membranes and vesicles, *Adv. Phys.*, **46** (1997), 13–137. https://doi.org/10.1080/00018739700101488
12. N. Mohandas, E. Evans, Mechanical properties of the red cell membrane in relation to molecular structure and genetic defects, *Annu. Rev. Biophys. Biomol. Struct.*, **23** (1994), 787–818. https://doi.org/10.1146/annurev.bb.23.060194.004035
13. A. Gruber, *Curvature Functionals and p-Willmore Energy*, Ph.D. Thesis, Texas Tech University, 2019.
14. B. Athukorallage, G. Bornia, T. Paragoda, M. Toda, Willmore-type energies and Willmore-type surfaces in space forms, *JP J. Geom. Topol.* **18** (2015), 93–108. http://doi.org/10.17654/JPGTNov2015_093_108
15. J. C. C. Nitsche, *Lectures on Minimal Surfaces, Vol. 1*, Cambridge University Press, 1989.

16. A. Gruber, E. Aulisa, Computational p-Willmore Flow with Conformal Penalty, *ACM Trans. Graphics*, **39** (2020), 1–16. https://doi.org/10.1145/3369387

17. N. Vaidya, H. Huang, S. Takagi, Correct equilibrium shape equation of axisymmetric vesicles, in *Integral Methods in Science and Engineering: Techniques and Applications*, Birkhäuser Boston, (2008), 267–276. https://doi.org/10.1007/978-0-8176-4671-4_30

18. F. Jülicher, U. Seifert, Shape equations for axisymmetric vesicles: A clarification, *Phys. Rev. E*, **49** (1994), 4728–4731. https://doi.org/10.1103/PhysRevE.49.4728

19. K. Gaurav, Shape equations of the axisymmetric vesicles, (2022), 1–20. Available from: https://home.iitk.ac.in/ kugaurav/projects/Shape_equations_of_the_axisymmetric_vesicles.pdf.

20. R. C. Gonzalez, M. Toda, I. Mladenov, On the Shape of Red Blood Cell, *J. Geom. Symmetry Phys.*, **72** (2025), 1–38. https://doi.org/10.7546/jgsp-72-2025-1-38

AIMS Press